Electron swarm parameters of the hydrofluoroolefine HFO1234ze

Originally published in:
Plasma Sources Science and Technology 25(4), https://doi.org/10.1088/0963-0252/25/4/045005

Electron swarm parameters of the hydrofluoroolefine HFO1234ze

A. Chachereau[1], **M. Rabie**[1], **C. M. Franck**[1]

[1]Power Systems and High Voltage Laboratories, ETH Zurich, Physikstr. 3, 8092 Zurich, Switzerland

E-mail: alisec@ethz.ch

Abstract. In this contribution, the electron swarm parameters of the hydrofluoroolefine HFO1234ze, systematic name 1,3,3,3-Tetrafluoro-1-propene, are experimentally investigated. The analysis of the electron avalanche current measured in a pulsed Townsend experiment yields the effective ionization rate coefficient, the electron drift velocity and the longitudinal electron diffusion coefficient. The subsequent ion current is analyzed as well, to obtain separately the ionization and attachment rate coefficients. Measurements in pure HFO1234ze at different pressures show that the effective ionization rate is strongly influenced by three-body attachment and the three-body attachment rate coefficient is derived.

PACS numbers: 00.00, 20.00, 42.10

Keywords: HFO1234ze, $C_3H_2F_4$, 1,3,3,3-Tetrafluoro-1-propene, swarm parameter, electron attachment, three-body attachment
Submitted to: *Plasma Sources Sci. Technol.*

Introduction

The hydrofluoroolefine HFO1234ze ($CF_3CH{=}CHF$) is a refrigerant gas which was proposed as a replacement to the hydrofluorocarbon R134a (CF_3CH_2F) with a lower global warming potential (GWP) [1]. Recently HFO1234ze also attracted attention as a potential alternative to SF_6 for gaseous high voltage insulation [2, 3, 4]. It has a similar molecular structure as hexafluoropropylene ($CF_3CF{=}CF_2$), which has a comparable electric strength to SF_6 [5, 6, 7]. It is expected that the electric strength of HFO1234ze is lower than that of 1-C_3F_6 but still substantial. Moreover, HFO1234ze has an extremely low global warming potential on a hundred years horizon (< 1), compared to 23'500 for SF_6 [8].

In the present work, the electron swarm parameters of pure HFO1234ze and of several diluted mixtures of HFO1234ze with N_2, CO_2 and Ar are investigated in a pulsed

Townsend experiment. Part of these measurements were used for making breakdown voltage predictions in HFO1234ze [9]. The results are available on the online database ETHZ [10].

In the first section, the experimental setup and the method for analysing the measured current are briefly described. The obtained electron swarm parameters are presented in section 2. The effective ionization rate coefficient, the electron drift velocity and the longitudinal electron diffusion coefficient are obtained in pure HFO1234ze at different gas pressures. At one of these pressures, the ion currents in pure HFO are recorded and analyzed to obtain separately the ionization and attachment rate coefficients. The swarm parameters are also obtained in several diluted mixtures of HFO1234ze with N_2, CO_2 and Ar at the total pressure of 10 kPa. In the third section of this work, the pressure dependence of effective ionization rate coefficient in pure HFO1234ze is investigated using a kinetic model for three-body electron attachment, and the electron attachment properties of HFO1234ze are discussed in view of the swarm parameters of the diluted mixtures of HFO1234ze with N_2, CO_2 and Ar.

1. Methods

1.1. Swarm experiment

The pulsed Townsend experimental setup used in this work has been described previously [11]. A short laser pulse (1.5 ns FWHM) releases about 10^7 electrons from a back-illuminated photocathode. The electron swarm drifts in a uniform electric field through a gap between two Rogowski type electrodes. The gap distance is varied in the range of 11 to 21 mm and the applied voltage is up to 40 kV. The measurements are made at room temperature, and in a pressure range of 2 to 45 kPa. The transport parameters depend on the reduced field strength E/N, given in Townsend ($1\,\mathrm{Td} = 10^{-21}\,\mathrm{Vm}^2$). Here, E is the electrical field strength and N is the number density of the gas. The displacement current I_{exp} of the charged particle swarm drifting in the gap is recorded and evaluated. Sample current measurements are shown in figure 1.

1.2. Electron and Ion swarm analysis

The current is measured on two different timescales, namely during the electron transit time and during the ion transit time, see figure 2. The electron-dominated current of the electron swarm released by the laser pulse is followed by a current that is dominated by the ions that were produced during the electron transit. Ions are about two to three orders of magnitude slower than electrons, the ion current amplitude is consequently lower and the ion transit longer. The details of the electron and ion swarm analysis used in this work can be found in the appendix. The electron current analysis yields the effective ionization rate ν_{eff}, the electron drift velocity v_{e} and the longitudinal electron diffusion coefficient D_{L}. The total ionization rate ν_{i} and the total attachment rate ν_{a} such that $\nu_{\mathrm{eff}} = \nu_{\mathrm{i}} - \nu_{\mathrm{a}}$, as well as the drift velocities for anions v_{n} and cations v_{p}, are

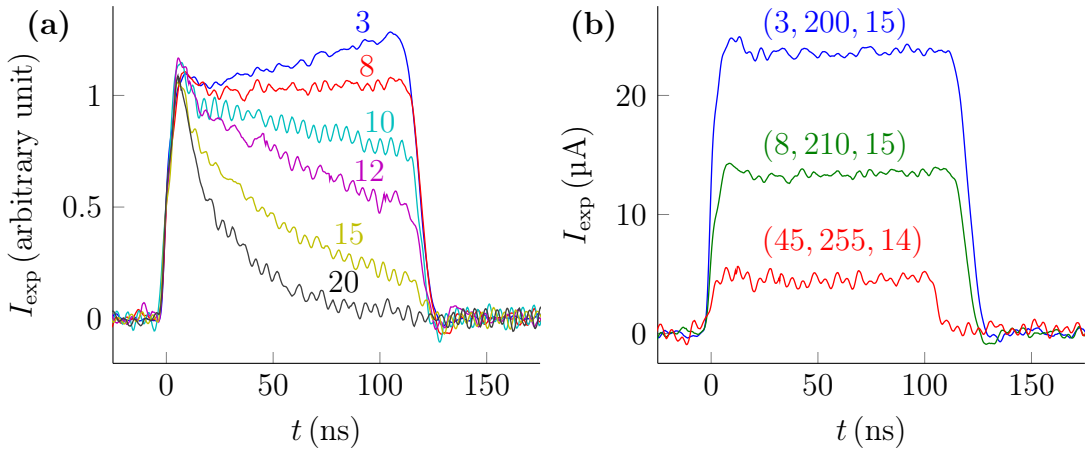

Figure 1: **(a)** Current versus time in HFO1234ze at $E/N = 210\,\text{Td}$, pressures of $3, 8, 10, 12, 15$ and $20\,\text{kPa}$ and for an electrode gap distance $d = 15\,\text{mm}$. The current is rescaled for easier comparison. **(b)** Current versus time in HFO1234ze in different conditions (p in kPa, E/N in Td, d in mm) chosen such that the effective ionization rate coefficient $k_{\text{eff}} \simeq 0$.

obtained from the subsequent ion current analysis. This approach considers one drift velocity for the anions v_{n} and one for the cations v_{p}, whereas the possible presence of additional ion species, reaction between species or clusters formation is not considered. In the case of several anions, as in the present work, v_{n} must be considered as an averaged drift velocity over all anion species.

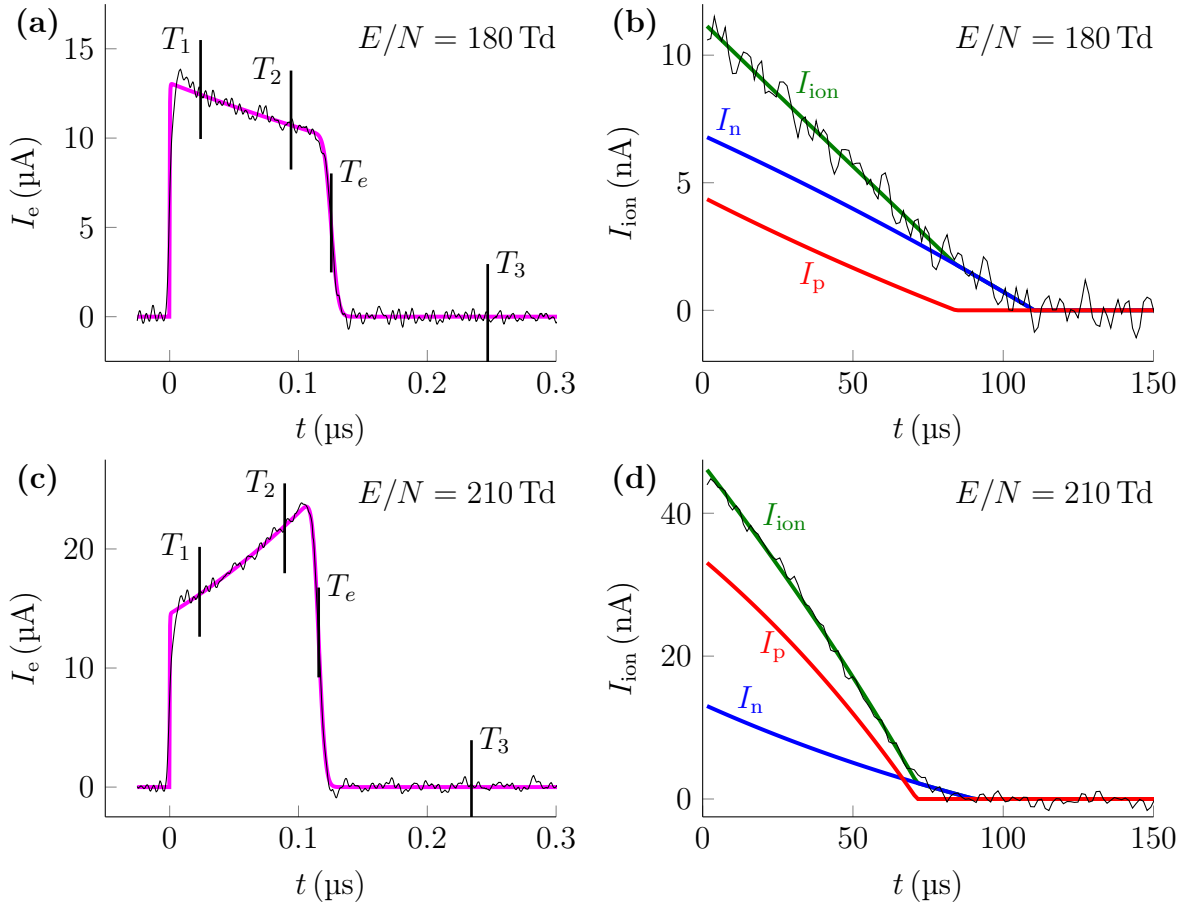

Figure 2: Current versus time in HFO1234ze at the pressure $p = 3$ kPa and for an electrode gap distance $d = 15$ mm. **(a)** Electron current and **(b)** ion current at $E/N = 180$ Td. **(c)** Electron current and **(d)** ion current in HFO1234ze at $E/N = 210$ Td. The thin lines are the measured currents whereas the thick lines correspond to the models of electron and ion swarms described in the appendix 3.4 and 3.5, in particular I_p is the positive ion current, I_n is the negative ion current and I_{ion} is the total ion current. The times T_1, T_2, T_3 and T_e are defined in the appendix 3.6

.

2. Results

2.1. HFO1234ze at different pressures

The effective ionization rate coefficient $k_{eff} = \nu_{eff}/N$ in HFO1234ze has been obtained at pressures ranging from 3 to 45 kPa. The values of k_{eff} are shown in figure 3 as a function of E/N. A strong pressure dependence of k_{eff} is observed over the whole E/N range. In particular, the density reduced critical electric field $(E/N)_{crit}$, for which k_{eff} equals zero, increases strongly with increasing gas pressure.

The electron drift velocity v_e and the density normalized longitudinal electron diffusion coefficient ND_L in HFO1234ze were obtained at pressures between 3 to 45 kPa

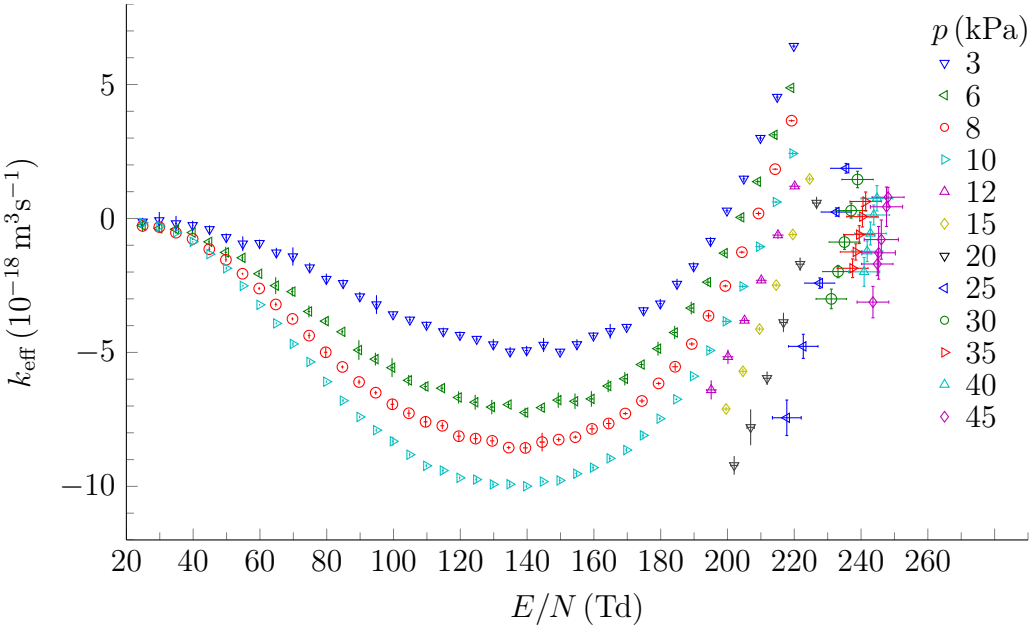

Figure 3: Effective ionization rate coefficient in HFO1234ze at different gas pressures as a function of E/N.

and found to be independent of the gas pressure. Figure 4 shows the average and the standard deviation of v_{e} and ND_{L} over the different pressures, as a function of E/N. The same quantities are shown for N_2, CO_2 and Ar for comparison.

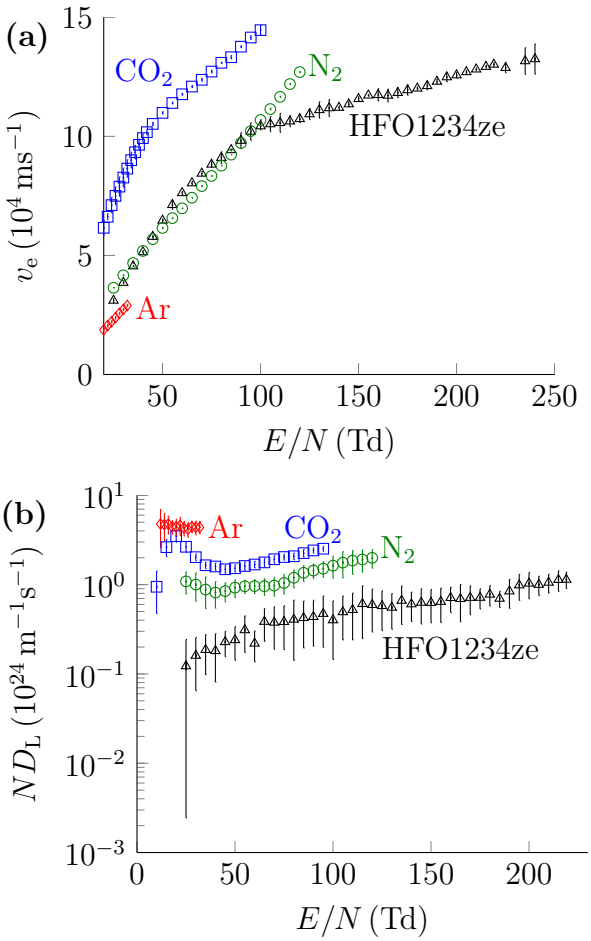

Figure 4: **(a)** Electron drift velocity v_e and **(b)** density normalized longitudinal electron diffusion coefficient ND_L in HFO1234ze, N_2, CO_2 and Ar as a function of E/N.

2.2. Separating ionization and attachment rate coefficients

At the pressure of 3 kPa, the ion currents in HFO1234ze were measured in addition to the electron currents. In contrast to the electron currents, the ion currents were obtained only for $E/N \geq 130$ Td, since for lower E/N they were too small for being measured with the present instruments. Using the method described in the appendix 3.4, the total ionization and attachment rate coefficients $k_i = \nu_i/N$ and $k_a = \nu_a/N$ are obtained, as well as the average cation and anion drift velocities v_p and v_n. The rate coefficients k_i and k_a are shown in figure 5 (a) and the ion drift velocities are shown in figure 5 (b). The total attachment rate coefficient k_a increases slightly over the E/N range 130 to 220 Td. The total ionization rate coefficient k_i starts increasing at about 150 Td, below this value too few positive ions are present to obtain their drift velocity. The crossing point between k_a and k_i corresponds to the density reduced critical electric field $(E/N)_{crit} \simeq 198$ Td at the pressure of 3 kPa.

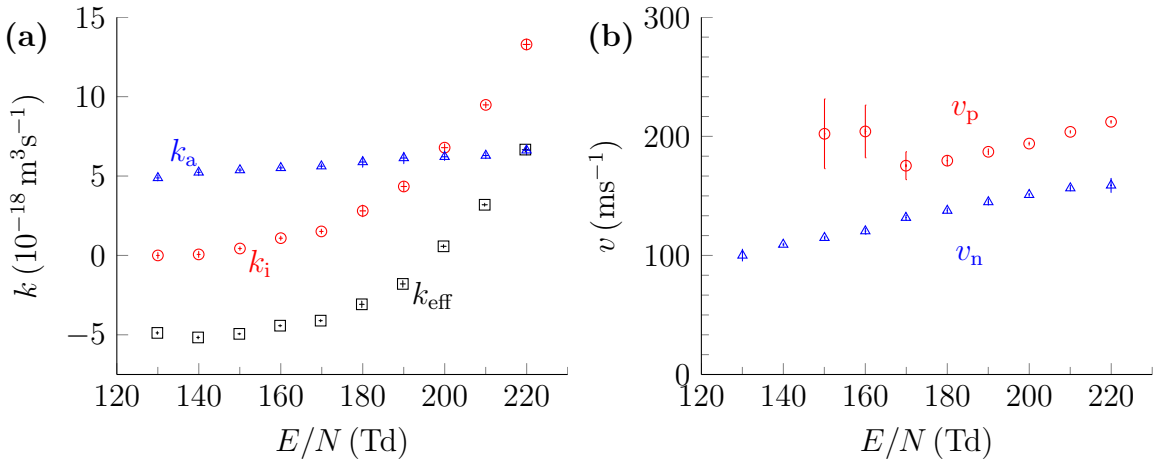

Figure 5: **(a)** Total attachment (k_a), total ionization (k_i), and effective ionization (k_eff) rate coefficients and **(b)** drift velocity of anions (v_n) and cations (v_p) in HFO1234ze at 3 kPa as a function of E/N.

2.3. Diluted mixtures of HFO1234ze in N_2, CO_2 and Ar

Figures 6, 7 and 8 show the swarm parameters of diluted mixtures of HFO1234ze in N_2, CO_2 and Ar respectively, compared to measurements in the pure buffer gases N_2, CO_2 and Ar. In the HFO1234ze/N_2 and HFO1234ze/CO_2 mixtures, only slight changes in the swarm parameters are observed compared to pure N_2 and CO_2. In the HFO1234ze/Ar mixtures, a strong change of the swarm parameters is observed compared to pure Ar. There is a strong increase in ionization in the HFO1234ze/Ar mixtures compared to pure Ar, but only weak electron attachment is observed in the HFO1234ze/Ar mixtures. The drift velocity in the HFO1234ze/Ar mixtures differs from that in pure Ar, and it increases with increasing percentage of HFO1234ze in the investigated mixtures. For the density reduced electric fields $E/N \geq 14$ Td in the mixture with 0.2% HFO1234ze, and for $E/N \geq 20$ Td in the mixture with 0.9% HFO1234ze, an after-current is observed after the electron transit which compromises the derivation of the electron drift velocity and the diffusion coefficient.

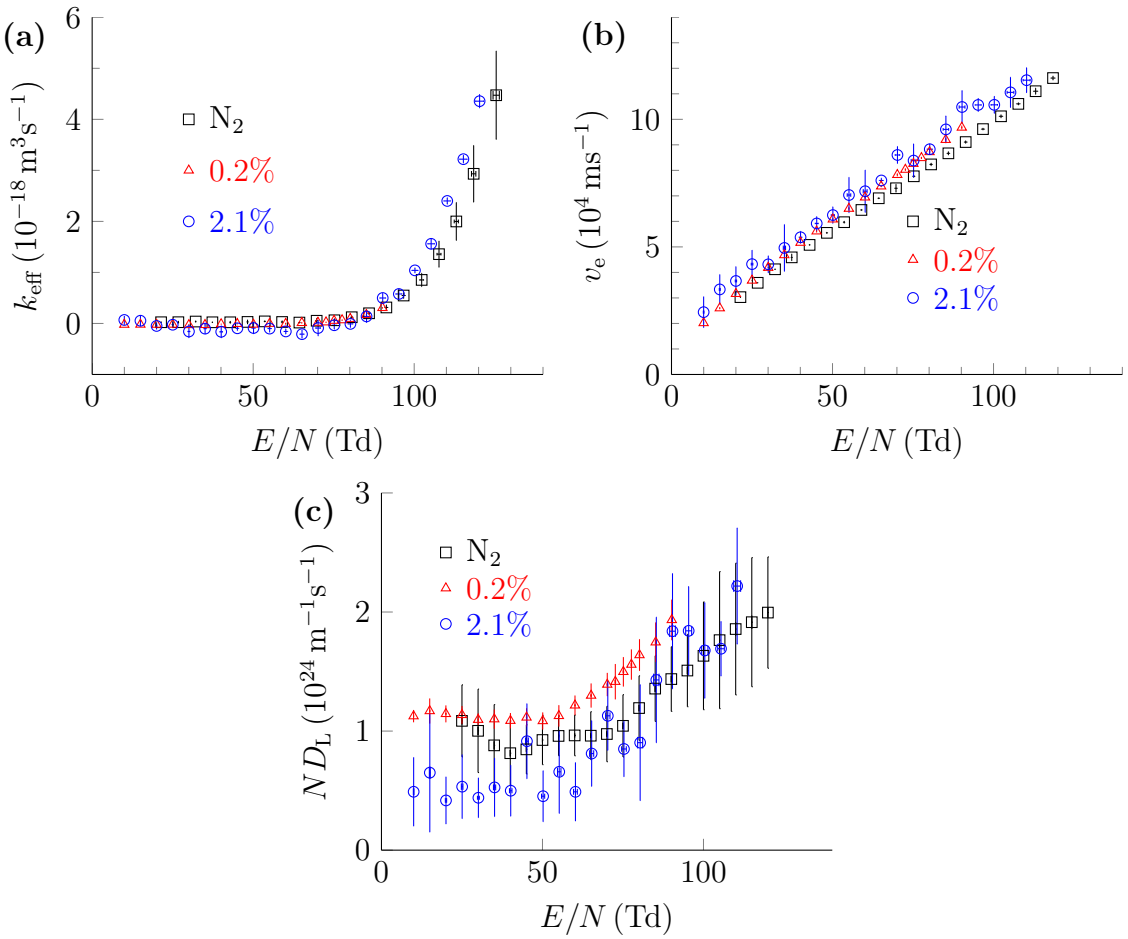

Figure 6: **(a)** Effective ionization rate coefficient, **(b)** electron drift velocity and **(c)** density normalized longitudinal electron diffusion coefficient in pure N_2 and in the mixtures of 0.2% and 2% HFO1234ze in N_2 as a function of E/N.

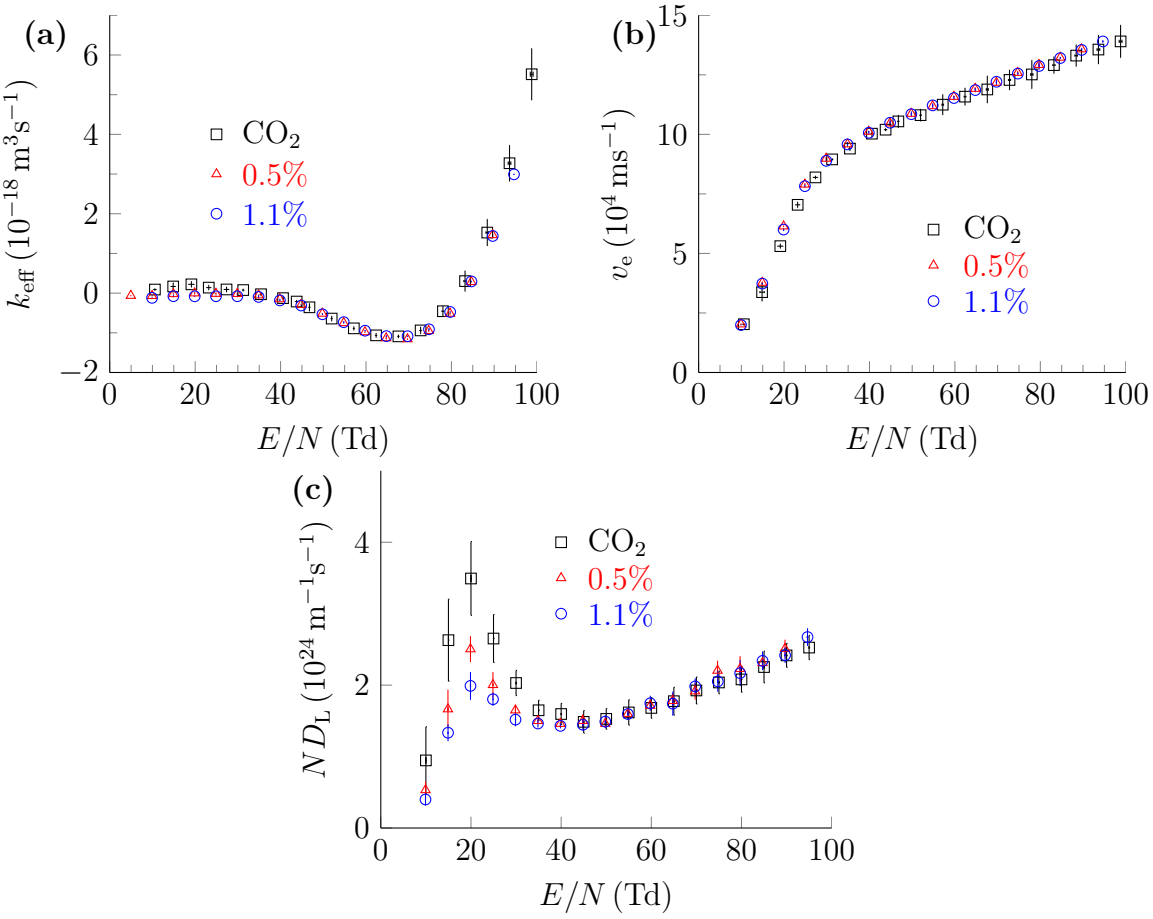

Figure 7: **(a)** Effective ionization rate coefficient, **(b)** electron drift velocity and **(c)** density normalized longitudinal electron diffusion coefficient in pure CO_2 and in the mixtures of 0.5% and 1.1% HFO1234ze in CO_2 as a function of E/N.

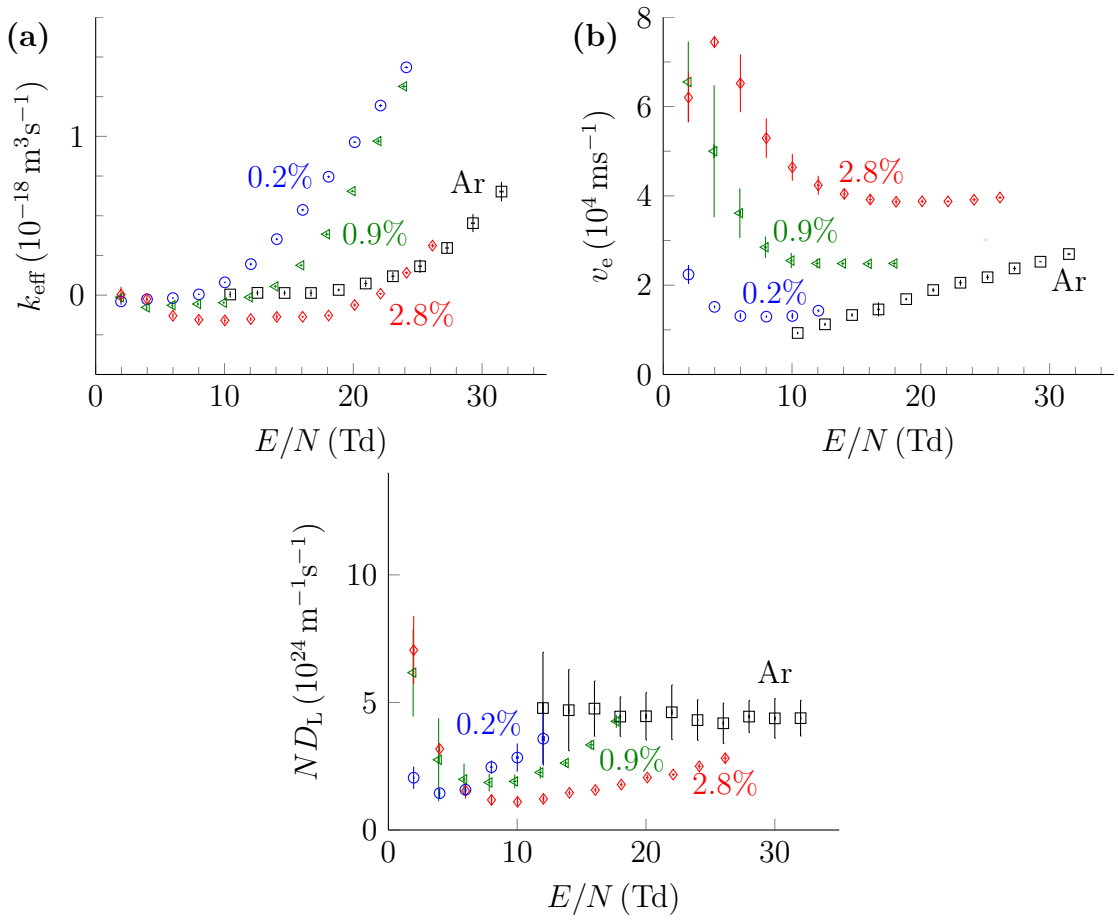

Figure 8: **(a)** Effective ionization rate coefficient, **(b)** electron drift velocity and **(c)** density normalized longitudinal electron diffusion coefficient in pure Ar and in the mixtures of 0.2%, 0.9% and 2.8% HFO1234ze in Ar as a function of E/N.

3. Discussion

3.1. Three-body electron attachment to HFO1234ze

The effective ionization rate coefficient k_{eff} in pure HFO1234ze is clearly decreasing with increasing gas pressure. This pressure dependence has been observed as well in 1-C_3F_6 [6] and other fluorocarbon gases [12, 13] and is typically due to the occurrence of three-body electron attachment [14]. In this section, we consider the simple model for three-body attachment described in [16] and apply it to the present measurements. The elementary attachment processes considered are the following

$$C_3H_2F_4 + e \xrightarrow{k_{\text{da}}} A^- + B \text{ (dissociative attachment)}, \tag{1}$$

$$C_3H_2F_4 + e \underset{\tau^{-1}}{\overset{k_{\text{at}}}{\rightleftarrows}} (C_3H_2F_4^-)^* \text{ (parent ion attachment)}, \tag{2}$$

$$(C_3H_2F_4^-)^* + C_3H_2F_4 \xrightarrow{k_{\text{stab}}} C_3H_2F_4^- + C_3H_2F_4 \text{ (collisional stabilization)}, \tag{3}$$

$$(C_3H_2F_4^-)^* + C_3H_2F_4 \xrightarrow{k_{\text{det}}} e + C_3H_2F_4 + C_3H_2F_4 \text{ (collisional detachment)}. \tag{4}$$

where k_{da} is the rate coefficient of dissociative attachment, k_{at} is the rate coefficient of $(C_3H_2F_4^-)^*$ formation; τ^{-1} is the autodetachment rate from $(C_3H_2F_4^-)^*$; k_{stab} and k_{det} are the rate coefficients of collisional stabilization of $(C_3H_2F_4^-)^*$ and of collisional detachment from $(C_3H_2F_4^-)^*$. Additionally, HFO1234ze is ionized with a total ionization rate coefficient k_{i} which includes dissociative and non-dissociative ionization.

This simple kinetic model is sufficient to reproduce the present experimental findings. Introducing additional kinetic processes involving for instance ion clusters cannot be justified based on these findings alone, but it is clear that such processes could occur. The problem of non-unicity of the kinetic model derived from swarm data is well known [15]. Complementary investigations of HFO1234ze based for instance on ion mass spectrometry would be required to establish with certitude the attachment mechanism to HFO1234ze as was done for 1-C_3F_6 [7].

Through the processes (2) and (4), the density of electrons is coupled with that of $(C_3H_2F_4^-)^*$. After a few τ, the growth of the electron number is exponential, with the rate [16, 17, 18]

$$\nu_{\text{eff}}(N) = (k_{\text{i}} - k_{\text{da}})N - \frac{k_{\text{at}}k_{\text{stab}}N^2}{\tau^{-1} + (k_{\text{det}} + k_{\text{stab}})N}, \tag{5}$$

If we note

$$N_{\text{sat}} = ((k_{\text{stab}} + k_{\text{det}})\tau)^{-1}, \tag{6}$$

$$k_{\text{quad}} = k_{\text{at}}k_{\text{stab}}\tau, \tag{7}$$

equation (5) becomes

$$\nu_{\text{eff}}(N) = (k_{\text{i}} - k_{\text{da}})N - \frac{k_{\text{quad}}N^2}{1 + N/N_{\text{sat}}}. \tag{8}$$

Two limiting cases of equation (8) can be identified by comparing the gas density N to the quantity N_{sat} [16]

(i) When $N \ll N_{\mathrm{sat}}$, equation (8) simplifies as

$$\nu_{\mathrm{eff}}(N) = (k_{\mathrm{i}} - k_{\mathrm{da}})N - k_{\mathrm{quad}}N^2, \tag{9}$$

and the three-body attachment rate increases quadratically with the gas density.

(ii) When $N \gg N_{\mathrm{sat}}$, equation (8) simplifies as

$$\nu_{\mathrm{eff}}(N) = (k_{\mathrm{i}} - k_{\mathrm{da}})N - k_{\mathrm{quad}}N_{\mathrm{sat}}N, \tag{10}$$

and the three-body attachment rate increases linearly with the gas density.

The quantity N_{sat} can be seen as a "saturation" density for three-body attachment. Indeed, when the gas density greatly exceeds N_{sat}, the autodetachment lifetime τ is much larger than the mean time for the unstable anion to collide with a third body ($\tau \gg ((k_{\mathrm{stab}} + k_{\mathrm{det}})N)^{-1}$), therefore, the unstable anion is systematically collisionally stabilized/detached whereas the autodetachment becomes irrelevant. In this case, three-body attachment appears outwardly as a two-body process, with the apparent two-body rate coefficient $k_{\mathrm{quad}}N_{\mathrm{sat}}$.

The present measurements of the effective ionization rate in HFO1234ze are clearly obeying equation (9), as shown for some sample E/N values in figure 9. Thus, they correspond to the case (i) where $N \ll N_{\mathrm{sat}}$. The quantities $(k_{\mathrm{i}} - k_{\mathrm{da}})$ and k_{quad} are obtained as the coefficients from the linear regression of $\nu_{\mathrm{eff}}(N)$ on N and N^2. The quantity N_{sat} cannot be obtained from the present measurements as it does not appear in equation (9). Examples of the regression of equation (9) for sample E/N values are shown in figure 9. The rate coefficients $(k_{\mathrm{i}} - k_{\mathrm{da}})$ and k_{quad} are shown in figure 10 (a)

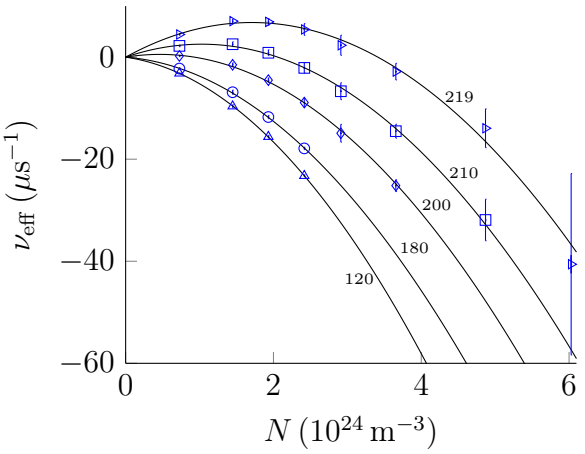

Figure 9: Measurements of ν_{eff} and regression with equation (9) for E/N of 120, 180, 200, 210 and 219 Td.

and (b). The three-body attachment rate k_{quad} reaches a maximum at 120 Td, then slowly decreases with increasing E/N.

The analysis developed here is independent from the ion current analysis that was presented in section 1.2. For comparison, the total attachment rate k_{a} that was obtained with the ion current analysis at the pressure $p = 3$ kPa would correspond here to

$$k_{\mathrm{a}}(N_1) = k_{\mathrm{da}} + k_{\mathrm{quad}}N_1, \tag{11}$$

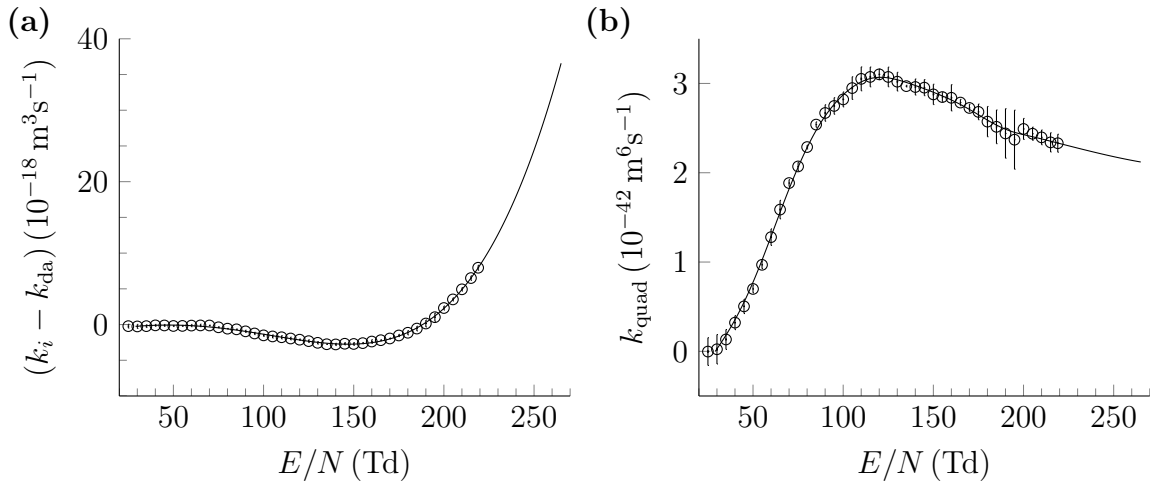

Figure 10: **(a)** Two-body rate coefficient $(k_\mathrm{i} - k_\mathrm{da})$ and **(b)** three-body attachment rate coefficient k_quad in HFO1234ze as a function of E/N. The points are determined using the regression (9), the lines are fits used in figure 11.

where N_1 is the gas number density at the pressure $p = 3\,\mathrm{kPa}$ and at room temperature.

Using the quantities $(k_\mathrm{i} - k_\mathrm{da})$ and k_quad, the rate coefficient k_eff can be calculated at different gas pressures with equation (9). These calculations are plotted in figure 11 at the same pressures where measurements in pure HFO1234ze were performed.

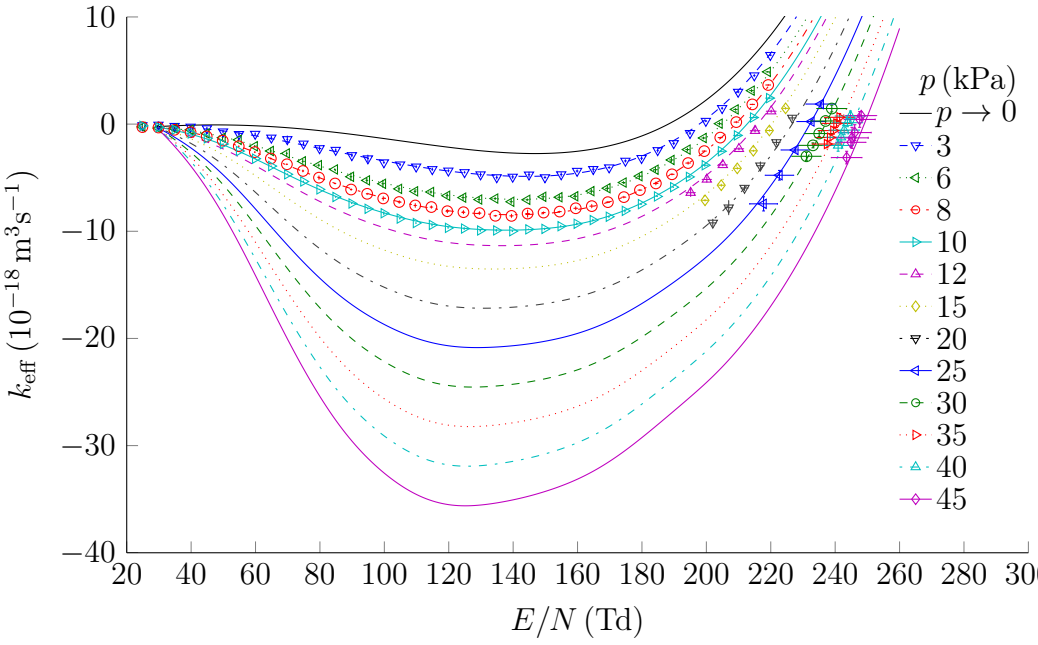

Figure 11: Effective ionization rate coefficient in HFO1234ze at different gas pressures as a function of E/N. The markers are measurement points that were presented in figure 3, whereas the lines are calculated from $(k_\mathrm{i} - k_\mathrm{da})$ and k_quad, in particular line for $p \to 0$ corresponds to the rate coefficient for two-body processes $(k_\mathrm{i} - k_\mathrm{da})$.

Since N_{sat} could not be obtained from the present measurements, it is uncertain up to which pressure the three-body attachment rate will continue increasing quadratically with the gas density following equation (9). At higher pressures, three-body attachment will eventually reach "saturation" and ν_{eff} will depend linearly on the gas pressure according to equation (10). Therefore equation (9) should not be used to extrapolate the present data towards higher gas pressures than where measured. However, the present considerations give the limit of k_{eff} towards low pressures, where three-body attachment is negligible. This limit corresponds to the term $(k_{\mathrm{i}} - k_{\mathrm{da}})$.

3.2. Diluted mixtures of HFO1234ze in N_2 and CO_2

The addition of small percentages of HFO1234ze in N_2 or CO_2 barely affects the effective ionization rate coefficient shown in figures 6 and 7, whereas pure HFO1234ze proved strongly electron attaching, with a density reduced critical electric field $\geq 188\,\mathrm{Td}$ as shown in figure 3. For strongly attaching gases, it is rather common to observe a strong change in k_{eff} relative to the pure buffer gas even in such diluted mixtures [18]. The absence of this change proves that, in the investigated E/N range, the attachment cross section of HFO1234ze has little overlap with the electron energy distribution functions in N_2 and CO_2. Thus, attachment to HFO1234ze would occur at relatively high electron energies. This is usually the case for dissociative electron attachment, but is less common for parent ion attachment.

3.3. Diluted mixture of HFO1234ze in Ar

The addition of a small percentage of HFO1234ze in Ar causes a strong change of the electron velocity at low E/N (see figure 8). At low E/N, the drift velocity in the HFO1234ze/Ar mixtures is decreasing with increasing E/N, and is higher than the drift velocity in either Ar or HFO1234ze. These phenomena, often referred to as negative differential mobility or negative differential conductivity, have been studied extensively [19, 21, 20] and are considered common for diluted mixtures of molecular gases in Ar.

The effective ionization rate coefficient is strongly affected by a small addition of HFO1234ze in Ar, see figure 8. For the most diluted mixture, which is 0.2% HFO1234ze in Ar, a strong increase of ionization relative to pure Ar is observed. The increase of ionization could be due to Penning ionization of HFO1234ze by metastable excited Ar states. Penning ionization could in addition account for the after-current observed in some of the electron transients in the mixtures of 0.2% HFO1234ze in Ar and 0.9% HFO1234ze in Ar in the higher E/N range. For the mixtures with 0.9% and 2.8% HFO1234ze, some electron attachment is observed which partially compensates the increase in ionization.

Conclusion

The electron swarm parameters of HFO1234ze were determined experimentally for the first time. The strong pressure dependence of the effective ionization rate coefficient was investigated assuming a three-body attachment mechanism to HFO1234ze. This model described well the observed pressure dependence of the effective ionization rate, and the three-body attachment rate was obtained. The two-body processes of ionization and attachment represent the limit of the effective ionization rate coefficient in HFO1234ze towards low pressures. The attachment to HFO1234ze at higher pressures would require further investigation, but the strong electron attachment observed already at relatively low pressures make HFO1234ze a promising gas for electric insulation at higher pressures. Since HFO1234ze would liquefy at the typical pressures used in high voltage gaseous insulation equipments, HFO1234ze mixtures with suitable buffer gases should be investigated as well.

Acknowledgments

This work is financially supported by ALSTOM Grid GmbH, Pfiffner AG and ABB Switzerland.

Appendix

3.4. Model of electron swarms

In our experiment, a voltage U is applied between two Rogowski type electrodes separated by a gap distance d, resulting in a homogenous electric field E in the gap. At time $t = 0$, a short laser pulse releases n_0 photo-electrons from a photocathode into the gas of number density N. The electron swarm drifts, after a very short non-equilibrium phase, constantly in the direction of the anode. The measured current is a consequence of the drift of all charged particles (electrons and ions) in the gap. For this situation, equations for the current from electrons or ions have been obtained previously [22, 23, 5]. The electron swarm model used here is based on a Gaussian spatial distribution of the swarm electrons and the corresponding electron current can be expressed for $t \geq 0$ as [11]

$$I_\mathrm{e}(t) = \frac{I_0}{2} \exp\left(\nu_\mathrm{eff} t\right) \left(1 - \mathrm{erf}\left(\frac{t - T_\mathrm{e}}{\sqrt{2\tau_\mathrm{D} t}}\right)\right), \tag{12}$$

$$I_0 = \frac{n_0 q_0}{T_\mathrm{e}}, \tag{13}$$

where q_0 is the electron charge, I_0 is the electron current at time $t = 0$, T_e is the drift time and ν_eff is the effective ionization rate. The canonical error function "erf" accounts for the absorption of the swarm at the anode. The characteristic time for longitudinal diffusion τ_D is related to the longitudinal diffusion coefficient D_L via $2D_\mathrm{L} = v_\mathrm{e}^2 \tau_\mathrm{D}$, where v_e is the electron drift velocity. The initial distribution of the released electrons is

assumed to be a Dirac delta. In case of strong electron detachment, cathodic feedback or photo-ionization by secondary photons, equation (12) cannot be used to derive precise values of v_e and τ_D from our measured currents. However, it can be still applied to derive ν_{eff}, as will be described in section 3.6.

3.5. Model of ion swarms

The total ion current is the sum of the currents arising from the drift of anions and cations. In this section, we assume that there is only one species of cations and one species of anions. Furthermore, we assume that the effective rate in equation (12) is given by the ionization minus the attachment rate $\nu_{eff} = \nu_i - \nu_a$.

3.5.1. During electron transit Ions are treated as immobile during the electron transit, since electron drift velocities typically exceed ion drift velocities by up to three orders of magnitude. The charge densities for electrons $\rho_e(x,t)$, cations $\rho_p(x,t)$ and anions $\rho_n(x,t)$ obey

$$\frac{d}{dt}\rho_p(x,t) = \nu_i \rho_e(x,t), \tag{14}$$

$$\frac{d}{dt}\rho_n(x,t) = \nu_a \rho_e(x,t). \tag{15}$$

The currents associated with electron, cations and anions are

$$I_{e,p,n}(t) = \frac{v_{e,p,n}}{d}\int_0^d \rho_{e,p,n}(x,t)dx \tag{16}$$

where $v_{e,p,n}$ are the electron, cation and anion drift velocities. Thus, the spatial integration of equations (14) and (15) over the electrode gap yields

$$\frac{d}{dt}I_p(t) = \nu_i \frac{v_p}{v_e} I_e(t), \tag{17}$$

$$\frac{d}{dt}I_n(t) = \nu_a \frac{v_n}{v_e} I_e(t), \tag{18}$$

It follows that the total ion current $I_{ion}(t) = I_p(t) + I_n(t)$ is given by

$$I_{ion}(t) = \left(\nu_i \frac{v_p}{v_e} + \nu_a \frac{v_n}{v_e}\right)\int_0^t I_e(t')dt'. \tag{19}$$

3.5.2. After electron transit For the calculation of the ion currents at times $t \geq T_e$ the ion charge densities at time $t = T_e$ are needed. To obtain them, a simpler model of the electron current during the interval $[0, T_e]$ is used than the one described in section 3.4. The diffusion of the electron swarm is set to zero, yielding the electron charge density

$$\rho_e(x,t) = n_0 \exp(\nu_{eff} t)\delta(x - v_e t). \tag{20}$$

According to equation (14) and (15) static cation and anion charge densities are created until time T_e. At time T_e, the ion charge densities in the gap are

$$\rho_p(x, T_e) = n_0 \frac{\nu_i}{v_e} \exp\left(\frac{\nu_{eff}}{v_e} x\right), \tag{21}$$

$$\rho_n(x, T_e) = n_0 \frac{\nu_a}{v_e} \exp\left(\frac{\nu_{eff}}{v_e} x\right). \tag{22}$$

After the electron transit, between T_e and the transit times $T_p = d/v_p$ and $T_n = d/v_n$ of cations and anions, the currents originating from positive and negative ions can be expressed as a function of time $t' = t - T_e$ [23]:

$$I_p(t') = \frac{q_0}{T_p} \int_{v_p t'}^{d} \rho_p(x, T_e) dx = I_0 \frac{T_e}{T_p} \frac{\nu_i}{\nu_{eff}} (e^{\nu_{eff} T_e} - e^{\nu_{eff} \frac{T_e}{T_p} t'}), \tag{23}$$

$$I_n(t') = \frac{q_0}{T_n} \int_{0}^{d - v_n t'} \rho_n(x, T_e) dx = I_0 \frac{T_e}{T_n} \frac{\nu_a}{\nu_{eff}} (e^{\nu_{eff} T_e (1 - \frac{t'}{T_n})} - 1). \tag{24}$$

3.6. Electron current analysis

3.6.1. Separation of the electron and ion contribution The measured current I_{exp} is the sum of the electron and ion currents. For analyzing the electron current on the basis of the swarm model from section 3.4 the pure electron current I_e is necessary. In this section, the method for extracting I_e from I_{exp} is described. For zero electron diffusion, all electrons arrive at the anode at the same time T_e. However, in case of diffusion some electrons arrive earlier and some delayed. Therefore, a time T_3 is defined, at which "nearly" all electrons arrived. We determine T_e from the measured current and we set $T_3 = 2 \cdot T_e$. For typical gap distances and pressures in our experiments T_e is two orders of magnitude larger than τ_D, that is $T_e/\tau_D \approx 10^2$. In this case, the electron current at time T_3 drops to $I_e(T_3)/I_0 \propto (1 - \mathrm{erf}\left(0.5\sqrt{T_e/\tau_D}\right)) \approx 10^{-12}$ of its initial current, according to equation (12). Thus, from this time point on, no more electrons are present and the measured current is only from ions $I_{exp}(T_3) = I_{ion}(T_3)$. There is no sensitivity of $I_{ion}(T_3)$ on the exact value of T_3, since $I_{ion}(t)$ is basically constant on the time scale of T_e. Using this considerations together with equation (19), the measured current can be written as

$$I_{exp}(t) = I_e(t) + \left(\nu_i \frac{v_p}{v_e} + \nu_a \frac{v_n}{v_e}\right) \int_0^t I_e(t') dt'. \tag{25}$$

The factor in front of the integral can be obtained by the constraint $I_e(T_3) = 0$, and equation (25) becomes

$$I_{exp}(t) = I_e(t) + \frac{I_{exp}(T_3)}{\int_0^{T_3} I_e(t') dt'} \int_0^t I_e(t') dt'. \tag{26}$$

This integral equation for I_e is solved iteratively by starting in zero order with $I_e^{(0)}(t) = I_{exp}(t)$ and applying the operation

$$I_e^{(i)}(t) = I_{exp}(t) - \frac{I_{exp}(T_3)}{\int_0^{T_3} I_e^{(i-1)}(t') dt'} \int_0^t I_e^{(i-1)}(t') dt' \tag{27}$$

until $I_e^{(i)}(t)$ converges.

3.6.2. Applying the electron swarm model to I_e The electron current I_e is evaluated on the basis of the electron swarm model from section 3.4 in order to obtain the electron drift velocity v_e, the characteristic time for longitudinal diffusion τ_D and the effective reaction rate ν_{eff}. The rate ν_{eff} and the initial current I_0 are determined by means of a linear regression of $\log(I_e)$ versus t in an interval $[T_1, T_2]$ where I_e is unaffected by diffusion, as shown in figure 2 (a). The electron drift time T_e and the characteristic time for longitudinal diffusion τ_D are determined from a fit of equation (12) to the falling edge of I_e in the interval $[T_2, T_3]$.

3.7. Ion current analysis

After the electron current analysis, the ion current is analyzed on the basis of the ion swarm model from section 3.5. In this section, we will write temporal parameters as vectors, since all currents will be treated as vectors for the fit routine. We seek a minimum number of fit parameters, in order to perform an efficient fit of the measured current $\mathbf{I}_{exp}$ to the ion current model. Here, the fit minimizes the L^2-norm $||\mathbf{I}_{exp}-\mathbf{I}_p-\mathbf{I}_n||$. At this point, the initial electron current I_0, the effective rate ν_{eff} and the time T_e are already known from the electron current analysis, see section 3.6. For the ion current analysis they are treated as constant terms. After eliminating ν_a by using $\nu_{eff} = \nu_i - \nu_a$, three unknown parameters remain: ν_i, T_p and T_n. Notice that $\mathbf{I}_p$ and $\mathbf{I}_n$ depend linearly on ν_i. We therefore rewrite the norm $||\mathbf{I}_{exp} - \mathbf{I}_p - \mathbf{I}_n||$, using equations (23) and (24), to the form $||\mathbf{a} - \nu_i\mathbf{b}||$, with [24]

$$\mathbf{a} = \mathbf{I} + I_0 \frac{T_e}{T_n}(e^{\nu_{eff}T_e(1-\frac{\mathbf{t}'}{T_n})} - 1) \ . \tag{28}$$

$$\mathbf{b} = I_0 \frac{T_e}{\nu_{eff}} \left(\frac{e^{\nu_{eff}T_e} - e^{\nu_{eff}\frac{T_e}{T_p}\mathbf{t}'}}{T_p} + \frac{e^{\nu_{eff}T_e(1-\frac{\mathbf{t}'}{T_n})} - 1}{T_n} \right) \ . \tag{29}$$

Thus, only two independent fit parameters, T_p and T_n, remain for the final fit, whereas the parameter ν_i that minimizes $||\mathbf{a}-\nu_i\mathbf{b}||$ is obtained by the linear inversion $\nu_i = \mathbf{a}\cdot\mathbf{b}/\mathbf{b}^2$, with the constraint $\nu_i \geq \nu_{eff}$.

3.8. Derivation of the electron drift velocity and diffusion coefficient

The electron drift time T_e and the characteristic time for longitudinal diffusion τ_D are in a first step obtained from fits to single current measurements, see section 3.6. One could derive the drift velocity simply by $v_e = d/T_e$. However, to increase precision, and to eliminate the possible offset in the initial swarm position or width due to the rather undefined non-equilibrium phase of the photo-electrons or experimental imprecision of the gap distance, the final values of v_e and τ_D are extracted from several measurement at the same E/N-value but different gap distances d. Figure 12 (a) shows electron currents,

measured at gap distances $\mathbf{d} = [d^{(1)}, d^{(2)}, d^{(3)}, d^{(4)}]$, which are fitted to derive the drift times $\mathbf{T}_\mathrm{e} = [T_\mathrm{e}^{(1)}, T_\mathrm{e}^{(2)}, T_\mathrm{e}^{(3)}, T_\mathrm{e}^{(4)}]$ as well as the characteristic time for longitudinal diffusions $\boldsymbol{\tau_\mathrm{D}} = [\tau_\mathrm{D}^{(1)}, \tau_\mathrm{D}^{(2)}, \tau_\mathrm{D}^{(3)}, \tau_\mathrm{D}^{(4)}]$. The values of τ_D should be equal but for the measurement uncertainty. The drift velocity is derived by linear regression of $\mathbf{d}$ versus $\mathbf{T}_\mathrm{e}$, corresponding to the slope in Figure 12 (b). Similarly, we obtain the final value for $\boldsymbol{\tau_\mathrm{D}}$ from linear regression of $\boldsymbol{\tau_\mathrm{D}}\boldsymbol{T_\mathrm{e}}$ versus $\mathbf{T}_\mathrm{e}$, as shown in Figure 12 (c).

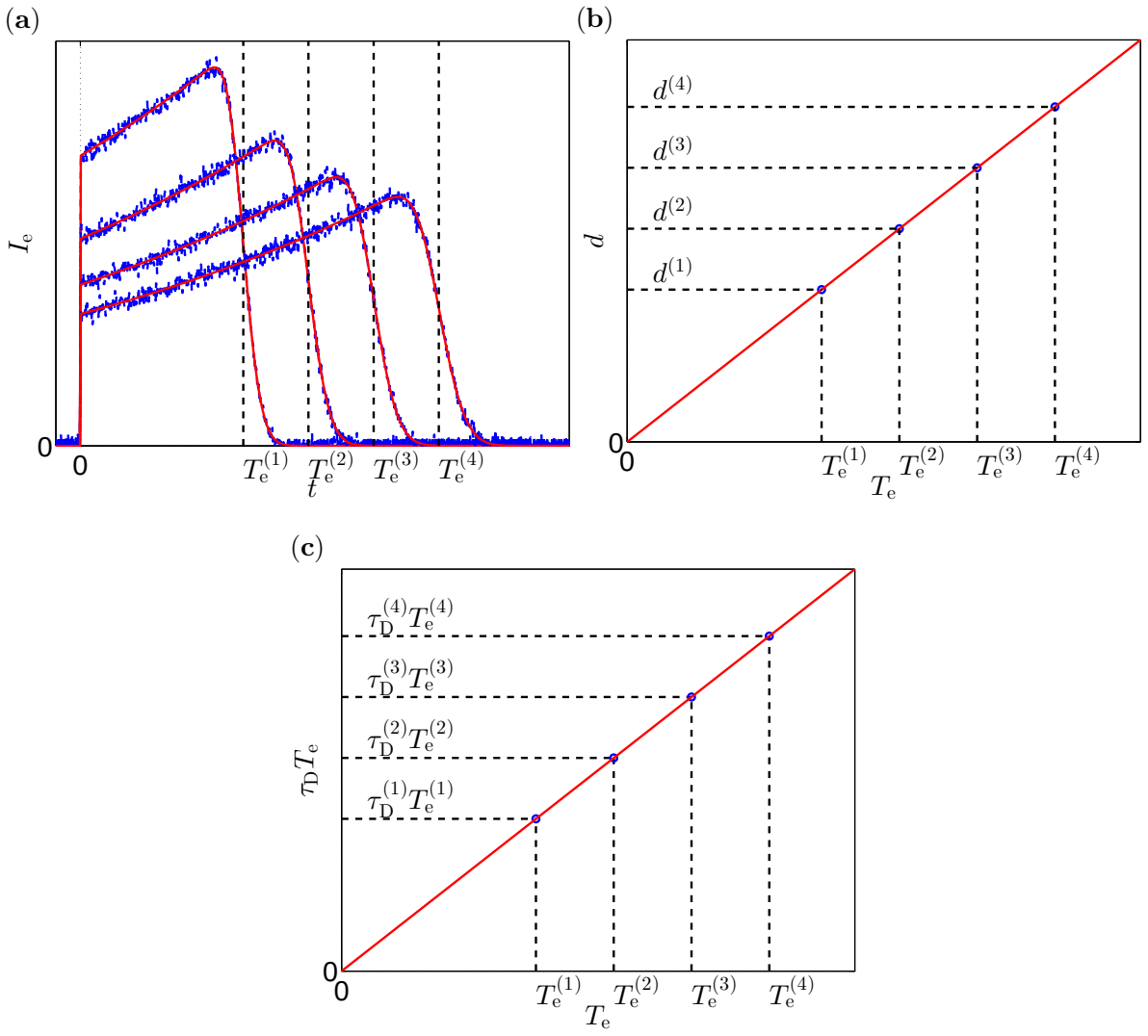

Figure 12: Sketch of how to obtain the electron drift velocity v_e and the characteristic time for longitudinal diffusion τ_D for measurements taken at the same E/N value. **(a)** Measured electron current I_e vs time for 4 different gap distances $d^{(1)}, d^{(2)}, d^{(3)}, d^{(4)}$ resulting in 4 drift times $T_\mathrm{e}^{(1)}, T_\mathrm{e}^{(2)}, T_\mathrm{e}^{(3)}, T_\mathrm{e}^{(4)}$. The full line is the fit of equation (12) to I_e. **(b)** Gap distance vs drift time (circles) for the electron currents from (a) and linear regression (full line). **(c)** Characteristic time for longitudinal diffusion multiplied by drift time $\tau_\mathrm{D} \cdot T$ vs drift time T (circles) from (a) and linear regression (full line).

3.9. Detection and correction of a gap distance offset

The exact value of the reduced electric field E/N as well as the derivation of v_e, as described in section 3.8, might be influenced by a possible inaccuracy of the measured gap distance d. The latter determines, together with the gap voltage U and the particle density N, the value $E/N = U/dN$. In the following we describe how to detect and determine a small offset d_0 in the measured value of d. Accordingly, we correct the value of E/N and the procedure of determining v_e from section 3.8. There we assumed that the measurements are exactly at the same E/N-value, see figure 12. However, if there is an offset d_0, those measurements are not exactly at the same E/N-value, but at

$$\boldsymbol{(E/N)_c} = \boldsymbol{E/N}\,(1 + d_0/\boldsymbol{d})\,. \tag{30}$$

We denote $(E/N)_c$ as the corrected, or real E/N-value. It follows, that the measured values of the drift velocity are not exactly equal, but

$$\boldsymbol{v_e} = (\mu N)\boldsymbol{(E/N)c}, \tag{31}$$

assuming that the reduced mobility μN is constant over a small E/N-interval. The linear relation bewteen d versus T_e, assumed in the section 3.8, must be replaced by

$$\boldsymbol{d} = d_0 + (\mu N)\boldsymbol{E/N}\,(1 + d_0/\boldsymbol{d})\,\boldsymbol{T_e}. \tag{32}$$

This equation for d_0 can be solved iteratively by starting in zero order with $d_0 = 0$ and applying the linear regression

$$\Delta d^{(i+1)} = \boldsymbol{d} - (\mu N)^{(i+1)}\boldsymbol{E/N}\left(1 + d_0^{(i)}/\boldsymbol{d}\right)\boldsymbol{T_e}. \tag{33}$$

where

$$d_0^{(i)} = \gamma \sum_{j=0}^{i} \Delta d^{(j)} \tag{34}$$

where γ is a damping parameter comprised in $]0, 1[$. We continue the iterations until $d_0^{(i)}$ converges. The final values of the distance offset d_0 and of the reduced mobility (μN) are obtained from the last iteration. Then, the final $\boldsymbol{(E/N)_c}$ values are obtained with equation (30). The final value of E/N that corresponds to the obtained reduced mobility (μN) is taken as the mean of the final $\boldsymbol{(E/N)_c}$ values.

References

[1] C. Hogue, Replacing the Replacements, *Chemical & Engineering News, 49 (89): 3132* (2011)

[2] M. H. Luly and R. G. Richard, Gaseous dielectrics with low global warming potentials, *United States Patent US 8 080 185 B2*, Honeywell International Inc (2011)

[3] Y. Kieffel and A. Girodet and D. Piccoz and R. Maladen, Use of a mixture comprising a hydrofluoroolefin as a high-voltage arc-extinguishing and/or insulating gas and high-voltage electrical device comprising same, *International Patent WO 2013/004798 A1*, Alstom Technology Ltd (2013)

[4] Y. Kieffel and A. Girodet and J. Porte, Medium- or high-voltage electrical appliance having a low environmental impact and hybrid insulation, *International Patent WO 2014/037566 A1*, Alstom Technology Ltd (2014)

[5] T. Aschwanden, Die Ermittlung physikalischer Entladungsparameter in Isoliergasen und Isoliergasgemischen mit einer verbesserten Swarm-Methode, *Diss. ETH Nr. 7931* (1985)

[6] S. R. Hunter, L. G. Christophorou, D. R. James and R. A. Mathis, Pressure-dependent electron attachment rates in perfluoroalkanes and perfluoropropylene (1-C3F6) and their effect on the breakdown strength of these gases, *Gaseous Dielectrics III, 7-20* (1982)

[7] S. R. Hunter, L. G. Christophorou, D. L. McCorkle, I. Sauers, H. W. Ellis and D. R. James, Anomalous electron attachment properties of perfluoropropylene (1-C3F6) and their effect on the breakdown strength of these gases, *J. Phys. D: Appl. Phys. 16, 573-580* (1983)

[8] G. Myhre, D. Shindell, F.-M. Bron, W. Collins, J. Fuglestvedt, J. Huang, D. Koch, J.-F. Lamarque, D. Lee, B. Mendoza, T. Nakajima, A. Robock, G. Stephens, T. Takemura and H. Zhang, *Anthropogenic and Natural Radiative Forcing. In: Climate Change 2013: The Physical Science Basis. Contribution of Working Group I to the Fifth Assessment Report of the Intergovernmental Panel on Climate Change [Stocker, T.F., D. Qin, G.-K. Plattner, M. Tignor, S.K. Allen, J. Boschung, A. Nauels, Y. Xia, V. Bex and P.M. Midgley (eds.)]. Cambridge University Press, Cambridge, United Kingdom and New York, NY, USA, p 731* (2013)

[9] M. Koch, C. M. Franck, High Voltage Insulation Properties of HFO1234ze, *IEEE Trans. Dielectr. Electr. Insul. accepted 28 April 2015*

[10] ETHZ database, www.lxcat.net.

[11] D. A. Dahl, T. A. Teich, C. M. Franck, Obtaining precise electron swarm parameters from a pulsed Townsend setup, *J. Phys. D: Appl. Phys. 45, 485201* (2012)

[12] J. Rademacher, G. Christophorou and R. P. Blaunstein, Electron Attachment to Sulphur Dioxide in High Pressure Gases, *J. Chem. Soc., Faraday Trans. 2 71, 1212-1226* (1975)

[13] S. R. Hunter, J. G. Carter and L. G. Christophorou, Electron attachment and ionization processes in CF4, C2F6, C3F8, and n-C4F10, *J. Chem. Phys. 86, 693* (1987)

[14] L. G. Christophorou and S. R. Hunter, Electrons in dense gases. In *Swarms of Ions and Electrons in Gases*. W. Lindinger, T. D. Mark and F. Howorka. Springer-Verlag (1984)

[15] Z. Lj. Petrovic., M. Suvakov, Z. Nikitovic, S. Dujko, O. Sasic, J. Jovanovic, G. Malovic and V. Stojanovic, Kinetic phenomena in charged particle transport in gases, swarm parameters and cross section data, *Plasma Sources Sci. Technol. 16 S1-S7* (2007)

[16] N. L. Aleksandrov, Three-body electron attachment to a molecule, *Usp. Fiz. Nauk 154, 177-206* (1988)

[17] S. M. Spyrou and L. G. Christophorou, Three-body electron attachment to a molecule, *J. Chem. Phys. 83, 2829* (1985)

[18] S. R. Hunter and L. G. Christophorou, Electron attachment to the perfluoroalkanes n-C_NF_{2N+2} (N =1-6) using high pressure swarm techniques, *J. Chem. Phys. 80, 6150* (1984)

[19] W. H. Long, Jr., W. F. Bailey, and A. Garscadden, Electron drift velocities in molecular-gas-rare-gas mixtures, *Phys. Rev. A. 13, 471* (1976)

[20] S. B. Vrhovac and Z. Lj. Petrovic, Momentum transfer theory of nonconservative charged particle transport in mixtures of gases: General equations and negative differential conductivity, *Phys. Rev. E 53, 4012* (1997)

[21] Z. Lj. Petrovic., R. W. Crompton and G. N. Haddad, Model Calculations of Negative Differential Conductivity in Gases, *Aust. J. Phys. 37, 23* (1984)

[22] J. Brambring, Der Stromverlauf einer Elektronenlawine mit Diffusion, *Z. Phys. 179, 532* (1964)

[23] H. Raether, Electron Avalanches and Breakdown in Gases, *London: Butterworths* (1964)

[24] M. Rabie, P. Haefliger and C.M.Franck, Obtaining electron attachment and ionization rates from simultaneous analysis of electron and ion swarms in a pulsed Townsend setup, *Conference Proceedings SPIG, 154* (2014)